Adsorption (2013) 19:631–641
DOI 10.1007/s10450-013-9486-7

Capillary condensation in mesoporous silica with surface roughness

Hideki Tanaka · Tatsumasa Hiratsuka · Natsumi Nishiyama · Kengo Mori · Minoru T. Miyahara

Received: 30 November 2012 / Accepted: 23 January 2013 / Published online: 5 February 2013

Abstract We construct an atomistic silica pore model mimicking templated mesoporous silica MCM-41, which has molecular-level surface roughness, with the aid of the electron density profile (EDP) of MCM-41 obtained from X-ray diffraction data. Then, we present the GCMC simulations of argon adsorption on our atomistic silica pore models for two different MCM-41 samples at 75, 80, and 87 K, and the results are compared with the experimental adsorption data. We demonstrate that accurate molecular modeling of the pore structure of MCM-41 by using the experimental EDP allows the prediction of experimental capillary evaporation pressures at all investigated temperatures. The experimental desorption branches of the two MCM-41 samples are in good agreement with equilibrium vapor–liquid transition pressures from the simulations, which suggests that the experimental desorption branch for the open-ended cylindrical pores is in thermodynamic equilibrium.

Keywords MCM-41 · Electron density profile · Surface roughness · Capillary condensation · Molecular simulation

1 Introduction

Templated mesoporous silica materials, such as MCM-41 (Kresge et al. 1992) and SBA-15 (Zhao et al. 1998), have attracted considerable attention because of their potential use as catalyst supports, as well as in separation, drug delivery, preparation of nanostructured materials, etc. (Corma 1997; Ciesla and Schuth 1999; Soler-Illia et al. 2002). These materials are also regarded as the most suitable model adsorbents for fundamental adsorption studies, because they have hexagonal arrays of cylindrical mesopores with narrow pore size distributions. Therefore, vapor–liquid phase transitions of fluids in the templated mesoporous silica materials have been extensively studied by experiments, theory, and molecular simulations (see a review by Gelb et al. 1999). In most theoretical and simulation studies, cylindrical pore models with smooth pore walls were used to represent the mesopores of MCM-41 and SBA-15 materials, and such molecular modeling has helped to understand the fundamental aspects of capillary condensation phenomena of fluids in mesopores (Ravikovitch et al. 1995; Ravikovitch et al. 1998; Neimark et al. 2000; Miyahara et al. 2000; Kanda et al. 2000a, 2000b; Neimark and Vishnyakov 2000; Ravikovitch et al. 2001; Vishnyakov and Neimark 2001; Neimark et al. 2003; Monson 2012). However, the cylindrical pore models with smooth pore walls cannot reproduce the surface adsorption behavior of fluids on MCM-41 and SBA-15 because of the presence of surface heterogeneities, originating from various surface hydroxyl groups, and morphological defects such as constrictions, microporosity, and surface roughness. In fact, recent experimental studies revealed the surface roughness on the pore walls of the MCM-41 and SBA-15 materials. Edler et al. (1997) modeled the pore wall structure of MCM-41 by using synchrotron X-ray diffraction data, which gives two-dimensional silica density profile projected on a basal plane. They showed that the pore wall of MCM-41 consisted of two distinct density regions: silica wall with high density, and corona with more diffuse form of silica between the cylindrical hole and the dense silica wall. The thickness of the diffuse silica wall was up to ca. 1 nm, and the existence of such region was

H. Tanaka · T. Hiratsuka · N. Nishiyama · K. Mori · M. T. Miyahara (✉)
Department of Chemical Engineering, Kyoto University, Katsura, Nishikyo, Kyoto 615-8510, Japan
e-mail: miyahara@cheme.kyoto-u.ac.jp

attributed to the corrugation of the pore wall or modulation of the pore center along the pore axis. Muroyama et al. (2006) developed a more sophisticated analytical formula of the crystal structure factor of MCM-41. They derived the formula by convoluting the Gaussian distribution function to a 2D crystal model of MCM-41 taking into account the surface roughness of the pore wall and obtained realistic electron density profile (EDP) of MCM-41 by fitting the analytical formula to the synchrotron X-ray diffraction data. In the case of SBA-15, similar but more refined models than those of Edler et al. (1997) were developed to determine the pore wall structure by using X-ray diffraction data (Imperor-Clerc et al. 2000; Hofmann et al. 2005). In these models for SBA-15, a corona with linearly increasing silica density was assumed, which is different from the model with stepwise silica densities by Edler et al. (1997). The thickness of the corona region determined by both authors was higher than 2 nm, which suggests that the surface roughness of SBA-15 is much higher than that of MCM-41. Then, Gommes et al. (2009) combined electron tomography (3D-transmission electron microscopy) and its image analysis to characterize the pore wall structure of SBA-15. In their analysis, the variations in the pore center and pore radius were added up, and the resulting amplitude of the pore wall corrugation was found to be 1.6 nm, which is in good agreement with the 1.9 nm thickness of the corona with linearly increasing silica density, obtained from the X-ray diffraction. These experimental facts suggest that the surface roughness of MCM-41 and SBA-15 is far higher than the length scale of the adsorbates.

After the pioneering work by Muroyama et al. (2006), the analytical formula of the crystal structure factor of MCM-41 was extended to deal with in situ synchrotron X-ray diffraction data for the argon adsorption on MCM-41 by Muroyama et al. (2008) and Miyasaka et al. (2009). The newly derived analytical formula gives not only the EDP of MCM-41 but also that of the adsorbed argon. Therefore, the authors compared the EDP of adsorbed argon from the in situ synchrotron X-ray diffraction data with that from so-called quenched solid density functional theory (QSDFT) developed by Ravikovitch and Neimark (2006), and confirmed good agreement between the EDPs of adsorbed argon from the experiments and QSDFT. In the QSDFT model, the pore wall of the templated mesoporous silica material is considered as a quenched component of the solid–fluid mixture with fixed density distribution, and the solid–fluid intermolecular interactions are split into a mean-field attractive part and a hard-sphere repulsive part expressed by multicomponent fundamental measure density functional (Rosenfeld 1989). This enables quantitative description of the adsorption on templated mesoporous silica materials with surface roughness, unlike the conventional nonlocal density functional theory (Tarazona 1985, Tarazona et al. 1987), which assumes regular smooth pore walls. However, the limits of applicability of the QSDFT method and its accuracy in the quantitative description of the adsorption on nanopores with surface roughness are still under discussion, and systematic comparison between the QSDFT calculations and molecular simulations is required.

Several methods for developing realistic molecular models for templated mesoporous silica materials have been reported, which include the method of reconstruction of O atoms alone or O and Si atoms in the silica pore wall artificially (Maddox et al. 1997; He and Seaton 2003) and the method of creation of tailor-made pores by carving out of a silica crystal block (Coasne and Pellenq 2004a, b; Sonwane et al. 2005; Coasne et al. 2006a; 2007; 2008a, b; 2010; Coasne and Ugliengo 2012). Another approach to model the templated mesoporous silica materials is to mimic the synthesis process by using molecular simulations. Coasne et al. (2006b), Hung et al. (2007), and Bhattacharya et al. (2009) constructed atomistic silica models for MCM-41 and SBA-15 by carving out of a silica cristobalite block with a mold, which is an assembly of micelles of coarse-grained surfactants, obtained by mesoscale-lattice Monte Carlo (MC) simulation (Siperstein and Gubbins 2003). The adsorption isotherms of noble gases on their atomistic silica pore models obtained by grand canonical Monte Carlo (GCMC) method, however, poorly coincided with experimental ones. This is attributed to the fact that one lattice unit in the lattice MC simulation is too large to reproduce the surface roughness at atomic length scales. Schumacher et al. (2006) developed the kinetic Monte Carlo (kMC) simulation to mimic the synthesis process of MCM-41 by using simplified interaction potentials and simplified representations of templating micelles. The kMC simulation follows the reaction path of the hydrothermal synthesis and calcination, and the resulting silica structure seemed to be quite realistic. They also performed GCMC simulations for the nitrogen adsorption on the MCM-41 model from kMC simulation at 77 K. Comparing the simulation and the experiment, the capillary condensation pressure from the simulation was much lower than that of the experiment, which suggests that the diameter of the templating micelle was too small. The pressure at which capillary condensation occurs is very sensitive to the pore size, and therefore, refinement of the model for the templating micelles would be required.

As stated above, the molecular modeling of the templated mesoporous silica materials is still a challenging task and more efforts should be devoted to reproduce the experimental trends, such as layering adsorption and

capillary condensation of fluids. The capillary condensation in the open-ended cylindrical pores of the templated mesoporous silica materials can be associated with hysteresis loop, and it is usually considered that the desorption branch corresponds to the thermodynamic equilibrium vapor–liquid phase transition, while the adsorption branch is due to the spontaneous phase transition from metastable state (Ravikovitch et al. 1995; Neimark et al. 2000; Neimark and Vishnyakov 2000). However, there is an argument that the adsorption branch represents the thermodynamic equilibrium, as opposed to many of the theoretical studies (Morishige et al. 1997; Morishige and Ito 2002; Morishige and Nakamura 2004; Morishige and Ishino 2007). The argument stems from the experimental evidence, where the plots of $T\ln(P/P_0)$ versus T for the capillary evaporation of nitrogen in several MCM-41 and SBA-15 samples vary linearly, and break at temperature T_h at which the hysteresis disappears, whereas the same plots for the capillary condensation show linear relationship over a wide temperature range, exceeding T_h. To settle the issue about the thermodynamic stabilities of capillary condensation and evaporation, precise molecular modeling of the templated mesoporous silica materials is indispensable.

In this study, we construct an atomistic silica pore model mimicking MCM-41, which has molecular-level surface roughness, with the aid of the EDP of MCM-41 obtained from X-ray diffraction data. Then, we present the GCMC simulations of argon in our atomistic silica pore models for two different MCM-41 samples at 75, 80, and 87 K, and the results are compared with the experimental adsorption data.

2 Experimental

Two MCM-41 samples synthesized with alkyltrimethylammonium bromides with different alkyl chain lengths (C16TAB and C18TAB) were used for the adsorption experiments, and they are designated as MCM-41-C16 and MCM-41-C18 in this study. The lattice parameters, a, obtained by X-ray powder diffraction measurements were $a = 4.161$ nm for MCM-41-C16 and $a = 4.975$ nm for MCM-41-C18. The adsorption isotherms of argon on two MCM-41 samples at 75, 80, and 87 K were measured by an adsorption apparatus consisting of a cryostat with a helium closed-cycle refrigerator and BELSORP-18 (BEL, Japan). The MCM-41 samples were outgassed at 423 K for 2 h under a pressure below 0.1 mPa, before each isotherm measurement. Exactly the same samples were used for the adsorption measurements at different temperatures without replacing the sample cell for reducing experimental errors. The cell temperature was kept within ±0.005 K during the adsorption measurements.

3 Computational methods

3.1 Modeling of MCM-41 mesoporous silica

3.1.1 Electron density profile of MCM-41

According to Muroyama et al. (2006, 2008), a 2D crystal model of MCM-41 can be defined as shown in Fig. 1a, where a is the distance between the circles which represent the cross-section of the cylindrical pores (the same with the lattice parameter of MCM-41) and c represents the portion of the pore to the length a. Thus, the pore diameter is given by ca ($0 \leq c \leq 1$). Then, to introduce the surface roughness of the pore wall, the following Gaussian distribution function $G(\mathbf{r})$ is convoluted to the crystal model of MCM-41:

$$G(\boldsymbol{r}) = \frac{1}{2\pi w^2 a^2} \exp\left(-\frac{|\boldsymbol{r}|^2}{2w^2a^2}\right) \tag{1}$$

where $\mathbf{r}$ is a position vector in 2D space perpendicular to the pore axis, and w is a fluctuation parameter. Hence, the relative EDP of MCM-41, $\rho^*(\mathbf{r})$, can be expressed as follows:

$$\rho^*(\boldsymbol{r}) = \int_{-\infty}^{\infty} C(\boldsymbol{r}')\, G(\boldsymbol{r}-\boldsymbol{r}')\, d\boldsymbol{r}' \tag{2}$$

where $C(\mathbf{r})$ is a function which represents the MCM-41 crystal, and $C(\mathbf{r}) = 0$ at the pore and $C(\mathbf{r}) = 1$ at the silica wall. Muroyama et al. (2008) constructed an analytical function of the structure factor $F(\mathbf{k})$, which is the Fourier transform of $\rho^*(\mathbf{r})$, and determined the parameters, $c = 0.8218$ and $w = 0.0699$, by fitting $|F(\mathbf{k})|^2$ to the structure factors obtained experimentally by synchrotron X-ray powder diffraction measurements for MCM-41. Figure 1b shows the EDP, which was calculated with Eq. (2) and the parameters $c = 0.8218$, $w = 0.0699$, and $a = 4.161$ nm. The $\rho^*(\mathbf{r})$ value was converted so that the EDP at the center of the pore wall coincides with the electron density of amorphous silica, $\rho_e = 652$ nm^{-3}.

3.1.2 Constructing atomistic MCM-41 model

In this study, the above-mentioned EDP was applied to construct an atomistic silica pore model mimicking MCM-41, which has molecular level surface roughness. First, we performed quench molecular dynamics simulation with BKS-type potential (Vanbeest et al. 1990) for constructing an amorphous silica block (density: 2.2 g/cm^3). The BKS potential is expressed as follows:

$$u(r_{ij}) = \frac{q_i q_j}{r_{ij}} + A_{ij}\exp(B_{ij}r_{ij}) - \frac{C_{ij}}{r_{ij}^6} \tag{3}$$

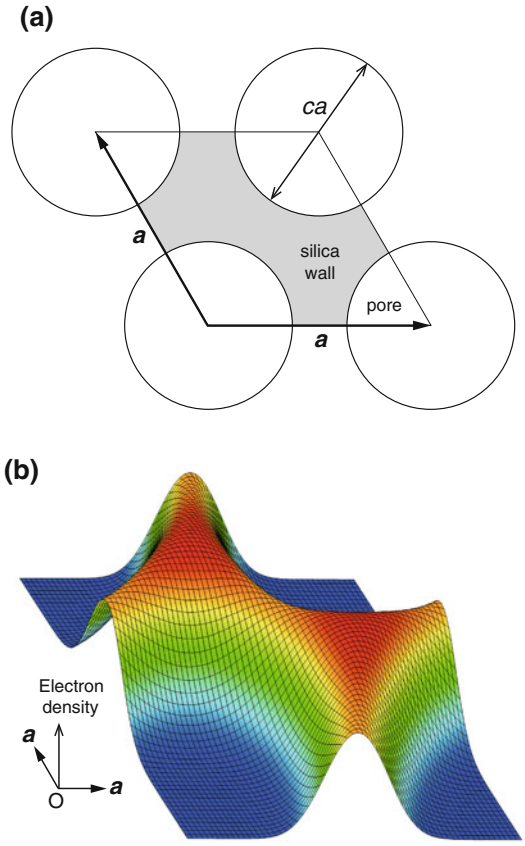

Fig. 1 **a** 2D crystal model of MCM-41: the *circles* represent mesopores and the shaded area is the silica wall. **b** Electron density profile of MCM-41

where r_{ij} is the distance between atoms, q_i is the atomic partial charge ($q_{Si} = 2.4e$ and $q_O = -1.2e$), and the values of parameters, A_{ij}, B_{ij}, and C_{ij} are listed in Table 1. The system was equilibrated in the canonical ensemble at 4,000 K, and subsequently, the fused silica was quenched from 4,000 K to room temperature at a rate of 0.23 K/fs. A time step of 0.7 fs was used to integrate the equations of motion. Periodic boundary conditions were applied in all three directions and full Ewald summation was used for the calculation of Coulombic interactions.

The obtained amorphous silica block was carved out to make a cylindrical pore, and then the pore wall was chipped away to coincide with the experimental EDP of MCM-41 by a MC method. In the MC scheme for shaping the pore wall, two trial moves were performed. One was the random removal of a Si atom, followed by the removal of the resulting unbonded Si and O atoms in the silica block. The second was the random regeneration of a Si atom, followed by the regeneration of dependent O atoms and checking of the connectivity to the silica framework. Then, the local number densities of Si and O atoms in the silica block, $\rho_{Si}(\mathbf{r})$ and $\rho_O(\mathbf{r})$, were calculated, subsequently a function representing electron cloud was convoluted to $\rho_{Si}(\mathbf{r})$ and $\rho_O(\mathbf{r})$. We used the following formula as the electron spread $s(\mathbf{r})$:

$$s(\boldsymbol{r}) = N_e\left(2\pi d^2\right)^{-3/2}\exp\left(-\frac{|\boldsymbol{r}|^2}{2d^2}\right) \tag{4}$$

where N_e is the number of electrons and d is the van der Waals diameter (0.42 nm for Si and 0.304 nm for O) (Miyasaka et al. 2009). This scheme was repeated to obtain good agreement between the experimental EDP of MCM-41 and the EDP obtained as the sum of the convolutions: $\rho_{Si}(\mathbf{r}) * s(\mathbf{r})$ and $\rho_O(\mathbf{r}) * s(\mathbf{r})$. Figure 2a shows the $\rho_{Si}(\mathbf{r})$ and $\rho_O(\mathbf{r})$ of the atomistic silica pore model in radial direction obtained by the MC scheme. The obtained EDP of the atomistic silica pore model is in reasonable agreement with the experimental EDP of MCM-41 (Fig. 2b).

Table 1 Parameters A_{ij}, B_{ij}, and C_{ij} for the BKS potential

	A_{ij} (eV)	B_{ij} (nm^{-1})	C_{ij} (10^{-6} eV nm^6)
O–O	1,388.773	27.6	175
Si–O	18003.7572	48.7318	133.5381

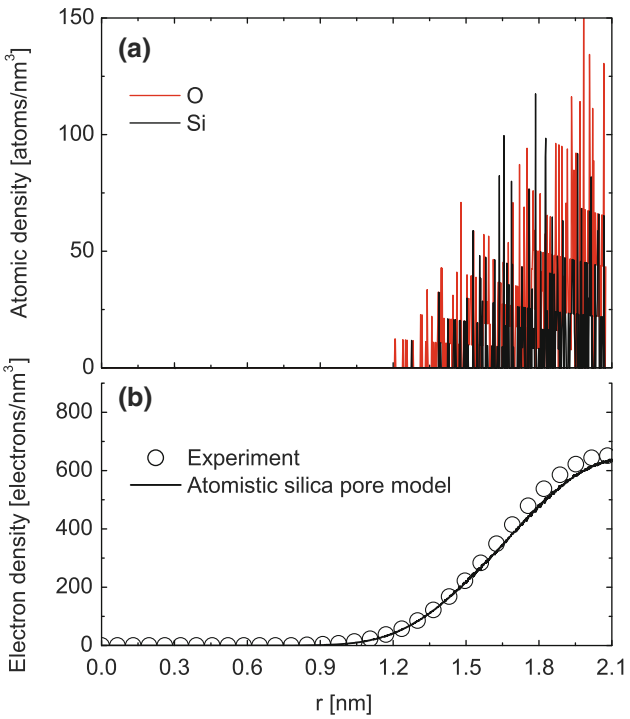

Fig. 2 **a** Local number density of O and Si atoms of the atomistic silica pore model in radial direction. **b** Comparison of electron density profile of the atomistic silica pore model with the experiment in radial direction

3.2 Thermodynamic integration (Peterson–Gubbins) method

The GCMC method is a powerful tool to simulate adsorption/desorption isotherm of fluids in nanopores. However, at subcritical temperatures, the GCMC method exhibits a hysteresis loop formed by discontinuous capillary condensation and evaporation branches and is not capable of determining the equilibrium phase transition between the vapor-like and liquid-like states. Therefore, the free energy of the system has to be calculated numerically to locate the thermodynamic coexistence point within the hysteresis loop. According to Peterson and Gubbins (1987), a grand thermodynamic potential Ω_A along a continuous adsorption isotherm N_A at temperature T_1 is calculated as follows:

$$\Omega_A(\mu, T_1) = -kT_1 N_A(\mu_{id}, T_1) - \int_{\mu_{id}}^{\mu} N_A(\mu', T_1)\, d\mu' \qquad (5)$$

where μ is a given chemical potential, and k is the Boltzmann's constant. The first term on the right-hand side is the grand thermodynamic potential at a chemical potential μ_{id}, which is sufficiently low so that the adsorption amount N_A at μ_{id} corresponds essentially to the ideal gas value. Then, the grand thermodynamic potential Ω_D along with the desorption isotherm at T_1 is calculated as:

$$\begin{aligned}\Omega_D(\mu, T_1) = &\frac{T_1}{T_2}\left[-kT_2 N_A(\mu_{id}, T_2) - \int_{\mu_{id}}^{\mu_c} N_A(\mu', T_2)\, d\mu'\right] \\ &+ T_1 \int_{1/T_2}^{1/T_1} [E_c(\mu_c, T) - N_c(\mu_c, T)\,\mu_c]\, d(1/T) \\ &- \int_{\mu_c}^{\mu} N_D(\mu', T_1)\, d\mu' \qquad (6)\end{aligned}$$

where T_2 is the temperature at which supercritical adsorption isotherm is obtained, N_c is the adsorption amount at constant chemical potential μ_c, E_c is the sum of the potential energy and the kinetic energy ($3NkT/2$) at μ_c, and N_D is the desorption isotherm at T_1. The Ω_D value is obtained by the integration along three reversible paths: the supercritical adsorption isotherm at T_2, the path $N_c(\mu_c, T)$ at μ_c, which connects the two isotherms at T_1 and T_2, and the desorption isotherm at T_1. Finally, a true phase equilibrium chemical potential, μ_{eq}, is determined as a point of intersection between the grand thermodynamic potentials, Ω_A and Ω_D. The constant chemical potential μ_c can be chosen arbitrarily if $\mu_{eq} < \mu_c$.

3.3 Grand canonical Monte Carlo simulations

Adsorption isotherms of Lennard-Jones (LJ) argon on the atomistic silica pore models at 75, 80, and 87.3 K were simulated by the GCMC method. The LJ parameters used in this study are $\sigma_{Ar-Ar} = 0.341$ nm and $\varepsilon_{Ar-Ar}/k = 119.8$ K for argon, and $\sigma_{O-O} = 0.2708$ nm, $\varepsilon_{O-O}/k = 101.6$ K, $\sigma_{Si-Si} = 0.0677$ nm, and $\varepsilon_{Si-Si}/k = 18.6$ K for the atomistic MCM-41 models (Bakaev et al. 1999). A cutoff distance was set to $5\sigma_{Ar-Ar}$. In the GCMC simulations, three trial movements, namely, displacement, creation, and deletion, were made with the same probabilities. The system was equilibrated for 2.5×10^7 MC steps, after which the data were collected for another 2.5×10^7 steps. The length of the Markov chain of 2.5×10^7 steps corresponds to more than 1.6×10^4 configurations per particle for all the cases investigated in this study. The final configuration was used as the initial state for the next simulation run.

By using the GCMC method, we also generated supercritical adsorption isotherm at $T_2 = 150$ K, and a path at the constant chemical potential μ_c to apply the thermodynamic integration method. We chose the $\mu_c/\varepsilon_{Ar-Ar}$ value (μ_c^*) of -9.142 at $T_1 = 75$ K, $\mu_c^* = -9.319$ at $T_1 = 80$ K, and $\mu_c^* = -9.682$ at $T_1 = 87$ K, and then, we performed the GCMC simulations with the respective chemical potentials at six different temperatures: 140, 130, 120, 110, 100, and 90 K.

Prior to the GCMC simulations, we computed chemical potentials for bulk fluid argon by averaging the Boltzmann factor of a test particle potential (Widom method) with the canonical MC method, and the pressure of the fluid, P, was obtained from the virial theorem. We employed 256 argon atoms for the MC simulations. A potential cutoff was set to $5\sigma_{Ar-Ar}$, and the standard long-range corrections were applied. Finally, the obtained chemical potentials were used as the input for the GCMC simulations. Then, the relative pressure, P/P_0 (P_0: saturated vapor pressure) was calculated with the vapor–liquid and vapor–solid coexistence curves of LJ fluid obtained by Agrawal and Kofke (1995) to compare the GCMC adsorption isotherms with the experimental ones.

4 Results and discussion

4.1 Effects of lattice structure of mesopores on adsorption

Figure 3a shows a snapshot of the atomistic silica pore model for MCM-41-C16 constructed with the structure parameters $a = 4.161$ nm, $c = 0.8218$, and $w = 0.0699$. The model has hexagonal lattice structure and is a cuboid

with the dimensions of $L_x = a$, $L_y = 2a$, and $L_z =$ 5.115 nm. We also built another silica pore model with tetragonal lattice structure (Fig. 3b), which is a cuboid and has the dimensions of $L_x = a$, $L_y = a$, and $L_z = 5.115$ nm. The model with the tetragonal lattice structure was also constructed with the structure parameters of $c = 0.8218$ and $w = 0.0699$, and therefore, the pore wall structure is the same with the atomistic silica pore model having the hexagonal lattice structure. We performed the GCMC simulations for the argon adsorption on the two atomistic silica pore models at 87 K. Representative simulation snapshots are shown in Fig. 3c, d, and the resulting GCMC adsorption isotherms are shown in Fig. 4. The adsorption isotherms were normalized according to the adsorption amount at $P/P_0 = 0.95$. The GCMC adsorption isotherms on the two models show a hysteresis loop formed by spontaneous condensation and evaporation transitions, and are in good agreement with each other over the full pressure range. This fact suggests that there are no considerable effects of the lattice structure of mesopores on the argon adsorption, that is, the fluid–fluid interactions beyond the pore walls are negligibly small. Herein, the atomistic silica pore models with the tetragonal lattice structure mimicking the pore wall structure of MCM-41-C16 and MCM-41-C18 are used for further discussions.

4.2 Effects of surface roughness on adsorption

Figure 5a and b show a comparison between the experimental adsorption isotherm of argon on MCM-41-C16 and the simulated one of the atomistic silica pore model obtained by the GCMC method in the monolayer-multilayer adsorption region at 87 K. We also simulated argon adsorption in a cylindrical pore with smooth structureless wall (smooth pore model) at 87 K by the GCMC method, and the resulting adsorption isotherm is also plotted in Fig. 5a, b for comparison. The interaction potential for a cylindrical pore derived by Peterson et al. (1986) was used as an argon-wall interaction potential for the smooth pore model. The interaction parameters used are $\sigma_{Ar-w} =$ 0.3055 nm, $\varepsilon_{Ar-w}/k = 166$ K, solid density of 59.82 nm^{-3}, and pore diameter of 3.6 nm (between the centers of the solid atoms), respectively. All the adsorption isotherms in Fig. 5a and b were normalized by using the monolayer capacities obtained by applying the BET analysis to the each adsorption isotherm. The adsorption isotherm of the atomistic silica pore model gradually rises from lower pressures and represents the experimental adsorption isotherm of MCM-41-C16 very well without any parameter adjustments. From the snapshots for the argon adsorption on the atomistic silica pore model (Fig. 6a–c), it is clear that the gradual increment in the adsorption isotherm is because argon adsorbs in the pits on the silica surface providing

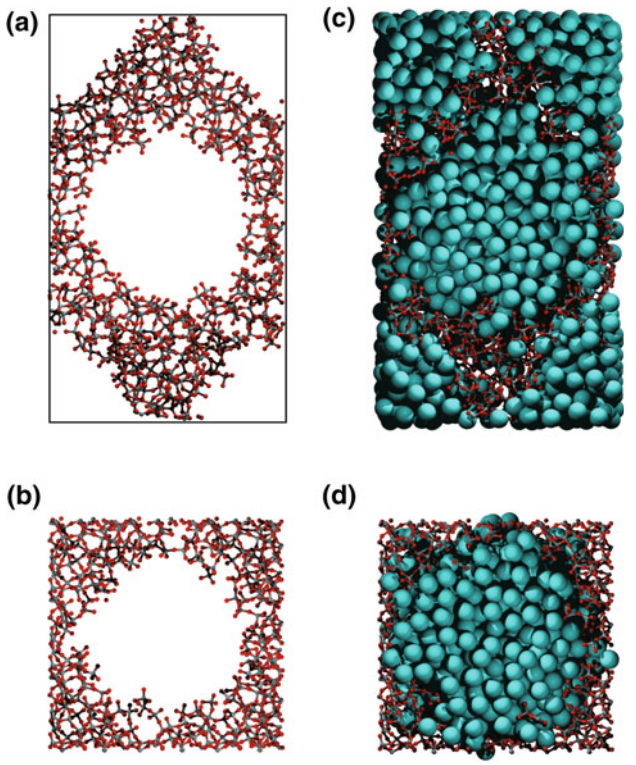

Fig. 3 Snapshots of atomistic silica pore models for MCM-41-C16: **a** hexagonal lattice model, **b** tetragonal lattice model. Representative simulation snapshots of argon adsorbed on the atomistic silica pore models for MCM-41-C16 at $P/P_0 = 1$: **c** hexagonal lattice model, **d** tetragonal lattice model

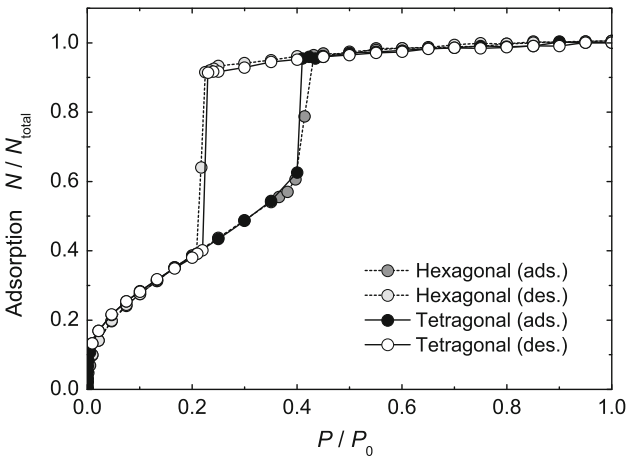

Fig. 4 Comparison of GCMC adsorption isotherms of argon on the atomistic silica pore models with hexagonal and tetragonal lattice structures at 87 K

strong solid–fluid interactions at low pressures. These facts suggest that our atomistic silica pore model appropriately reproduces the surface roughness of MCM-41-C16. On the other hand, the smooth pore model gives a sharp adsorption step and shows significant deviations from the experimental isotherm in the low-pressure region. This is due to the

cooperative monolayer formation of argon on the uniform surface of the smooth pore model (see snapshots in Fig. 6d–f), which is prevented on the heterogeneous surface of MCM-41.

To investigate the effects of surface roughness on the capillary condensation, we constructed several atomistic silica pore models, which have different surface roughness, as shown in Fig. 7a. In this case, for simplicity, we assumed a linear ramp of the atomic density of silica wall in the radial direction to represent the surface roughness, and we defined the width of the ramp as the roughness parameter δ. Then, the pore radius R was defined as the distance between the pore axis and the middle of the ramp, and it was set at the same value ($R = 1.8$ nm) for all the atomistic silica pore models. Figure 7b shows the simulated adsorption isotherms of argon for the atomistic silica pore models by the GCMC method at 87 K, which consist

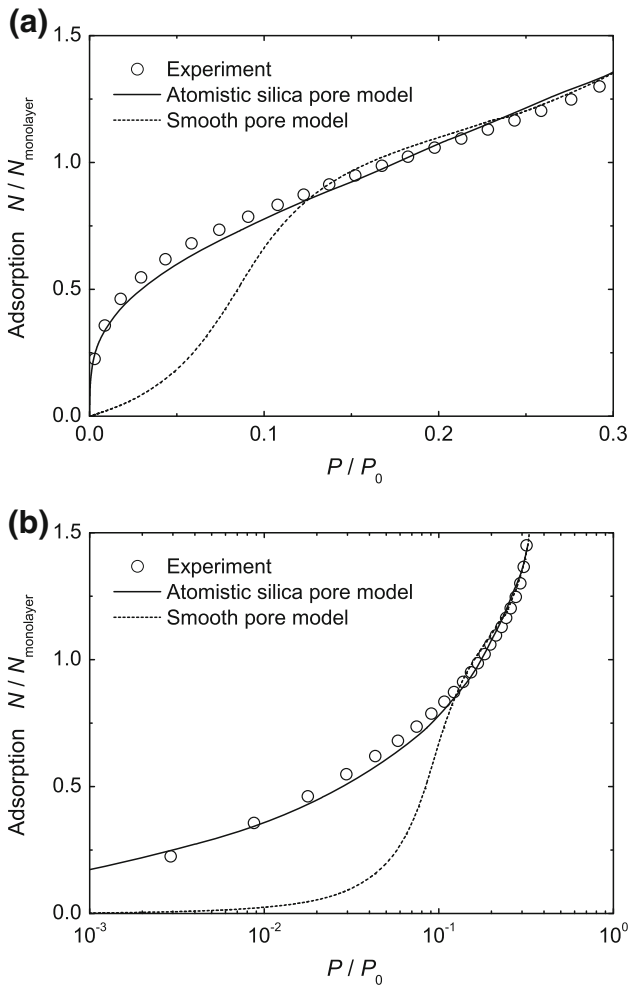

Fig. 5 Comparison between the experimental adsorption isotherm of argon on MCM-41-C16 and the simulated ones on the atomistic silica pore model and smooth pore model obtained by GCMC method in monolayer-multilayer adsorption region at 87 K

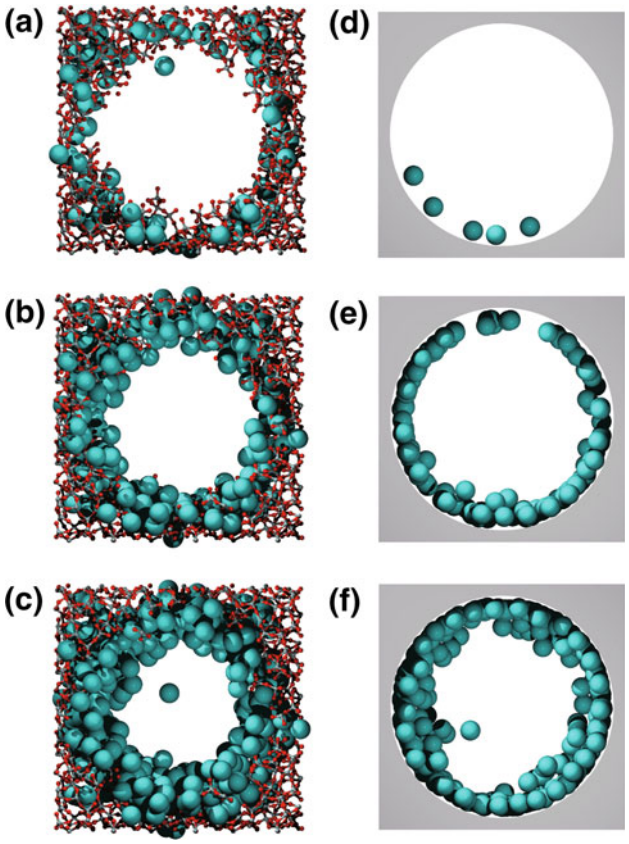

Fig. 6 Representative simulation snapshots for the argon adsorption (87 K) on the atomistic silica pore model at **a** $P/P_0 = 0.01$, **b** $P/P_0 = 0.1$, and **c** $P/P_0 = 0.3$, and on the smooth pore model at **d** $P/P_0 = 0.01$, **e** $P/P_0 = 0.1$, and **f** $P/P_0 = 0.3$

only of thermodynamically stable states including the equilibrium condensation transition by omitting metastable states and spontaneous adsorption/desorption transitions. The equilibrium transition pressures were determined by the Peterson and Gubbins method. With increasing δ value, the equilibrium condensation pressure decreases, though the pore radius was set at the same size. This suggests that the surface roughness affects the capillary condensation pressure to a considerable extent, and strongly indicates the importance of proper reproduction of the molecular-level heterogeneity of the pore wall for modeling the capillary condensation in MCM-41.

4.3 Capillary condensation in MCM-41: comparison with experiment

Figure 8a–c show the comparisons between the experimental adsorption isotherms of argon on MCM-41-C16 and the simulated ones on the atomistic silica pore model ($a = 4.161$ nm, $c = 0.8218$, and $w = 0.0699$) obtained by the GCMC method at 75, 80, and 87 K. All the adsorption isotherms were normalized according to the adsorption

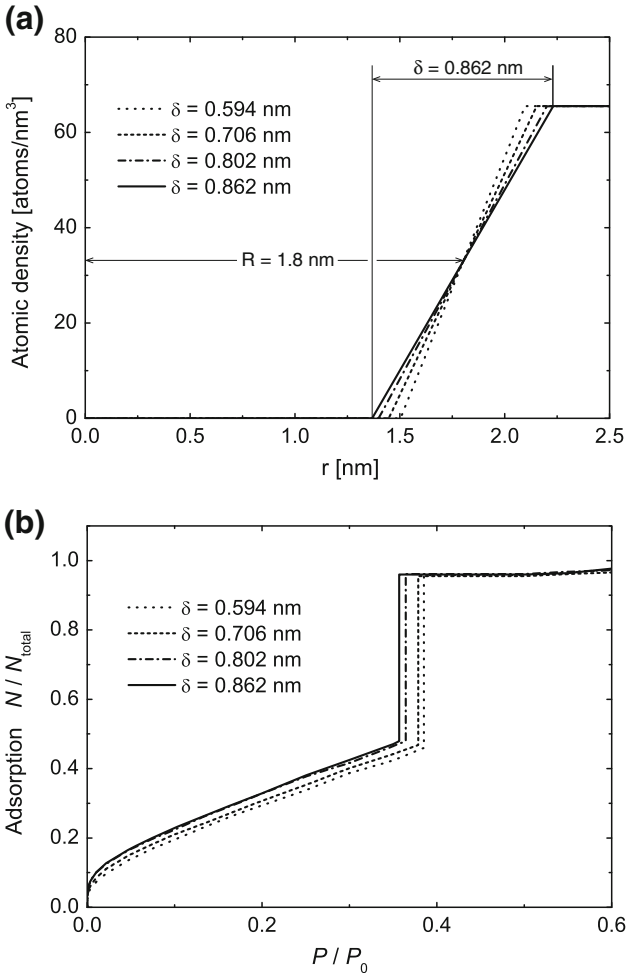

Fig. 7 **a** Atomic density profiles of the atomistic silica pore models in radial direction. $R = 1.8$ nm is the distance from the pore axis to the middle of the ramp, and δ is the width of the ramp as the roughness parameter. **b** Simulated adsorption isotherms of argon on each atomistic silica pore model obtained by GCMC method at 87 K. The adsorption isotherms only pass through thermodynamically stable states

amount at $P/P_0 = 0.95$. The simulated adsorption isotherms show a hysteresis loop, which corresponds to the spontaneous condensation and evaporation, and therefore the equilibrium transition pressures for the respective systems were determined by the Peterson and Gubbins method. In the case of the experimental result for MCM-41-C16 at 87 K (Fig. 8c), the adsorption isotherm is reversible (no adsorption hysteresis), and the capillary condensation/evaporation pressures coincide with the simulated equilibrium transition pressure. Then, the experimental adsorption isotherms of MCM-41-C16 at 75 and 80 K (Fig. 8a, b) show hysteresis, and the desorption branches are also in good agreement with the simulated equilibrium transition pressures. Namely, the simulated adsorption isotherms via the thermodynamic stable states at all the temperatures are in good agreement with the corresponding experimental desorption isotherms over the entire range of pressures. These facts suggest that the atomistic silica pore model appropriately reproduces the pore structure of MCM-41-C16, and the experimental desorption branch for MCM-41-C16 is due to the equilibrium evaporation, but the experimental adsorption branch comes from spontaneous condensation. However, there are large differences in the adsorption branch between the experiment and simulation at all the adsorption temperatures. This may be because the energy fluctuation of the experimental system is lager than that of the GCMC simulation, and therefore a transient state between the vapor-like and liquid-like states can be easily overcome at a lower pressure. In relation to this, we think that the experimental adsorption isotherm for MCM-41-C16 at 87 K can be reversible because the energetic barrier separating the vapor-like and liquid-like states at thermodynamic equilibrium is smaller than the energy fluctuation of the system, and thus the equilibrium transition can occur on the experimental adsorption process. The modeling of the spontaneous condensation on the

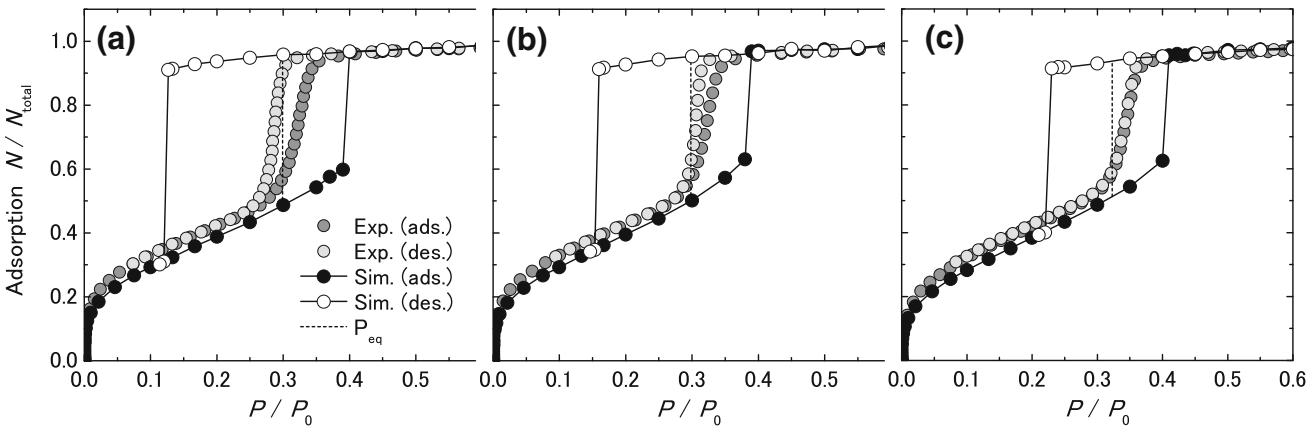

Fig. 8 Comparison between the experimental adsorption isotherms of argon on MCM-41-C16 and the simulated ones on the atomistic silica pore model obtained by GCMC method at **a** 75 K, **b** 80 K, and **c** 87 K. P_{eq} is the equilibrium transition pressure for the simulated adsorption isotherms determined by the Peterson and Gubbins method

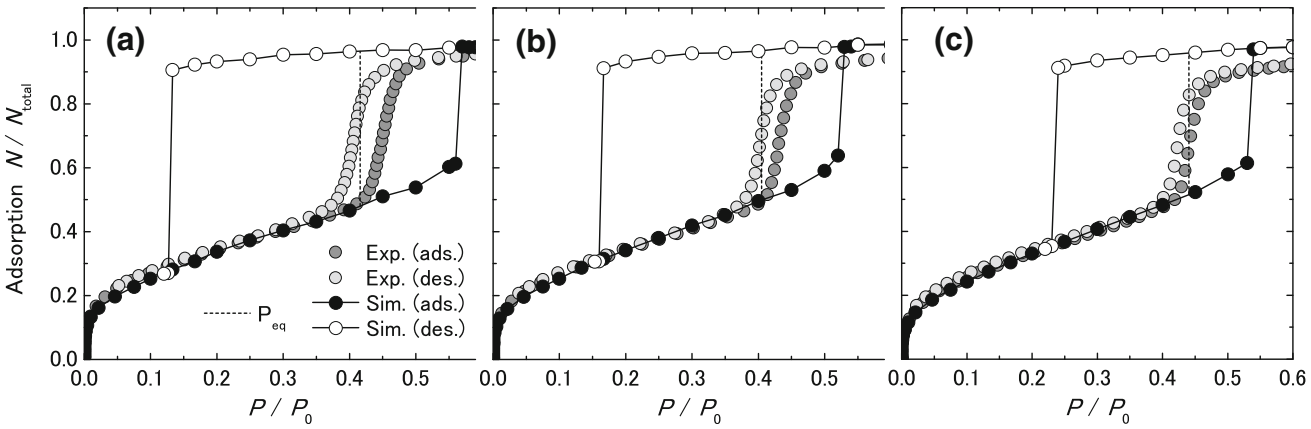

Fig. 9 Comparison between the experimental adsorption isotherms of argon on MCM-41-C18 and the simulated ones on the atomistic silica pore model obtained by GCMC method at **a** 75 K, **b** 80 K, and **c** 87 K. P_{eq} is the equilibrium transition pressure for the simulated adsorption isotherms determined by the Peterson and Gubbins method

adsorption process is our next subject, and the study is ongoing. Then, the spontaneous evaporation pressure of the simulated desorption branch is far lower than the experimental desorption (simulated equilibrium transition) pressure. This is because the atomistic silica pore model is infinite in length along the pore axis due to the periodic boundary condition. The spontaneous evaporation pressure should be much closer to the equilibrium transition pressure if the atomistic silica pore model is finite in length and open-ended.

We also constructed an atomistic silica pore model mimicking MCM-41-C18, with parameters $a = 4.975$, $c = 0.8218$, and $w = 0.0699$. In Fig. 9a–c, the simulated adsorption isotherms of argon on the atomistic silica model obtained by the GCMC method at 75, 80, and 87 K are compared with the experimental isotherms of MCM-41-C18. Similarly to MCM-41-C16, the simulated adsorption isotherms at all the temperatures agree well with the corresponding experimental ones, and the experimental desorption branches coincide with the simulated equilibrium transition pressures. These results suggest that our technique for constructing the atomistic silica pore model is critically useful in the modeling of the capillary condensation of fluids in the mesopores of MCM-41.

5 Conclusions

We have demonstrated that the accurate modeling of the structure of silica mesopores in MCM-41 by using the experimental EDP, which is a consistent modeling method in both theoretical and experimental points of view, allows the prediction of the experimental adsorption behavior of argon on MCM-41. We have gained insight into the role that the surface roughness plays in determining the adsorption behavior of argon on MCM-41 by using GCMC simulations. In general, we found that the surface roughness of the atomistic silica model affects both the monolayer-multilayer adsorption and the capillary condensation pressure of argon at subcritical temperatures. The experimental desorption branches of MCM-41-C16 and MCM-41-C18 were in good agreement with the simulated equilibrium transition pressures, and this suggests that the experimental desorption branch represents thermodynamic equilibrium. However, a large difference in the adsorption branch between the experiment and simulation was observed for all the cases. This finding suggests that the energy fluctuation to overcome the activation barrier for the transition from vapor-like state to liquid-like state is different between the experiment and the GCMC simulation. The modeling of the spontaneous condensation of fluids in the atomistic silica pores is in progress, and the results will be reported in the near future.

Acknowledgments The authors are grateful to Prof. A. Matsumoto of Toyohashi University of Technology, Prof. T. Okubo, Prof. A. Shimojima, and Dr. M. Kubo of The University of Tokyo, for donating the MCM-41 samples. H. T. thanks Dr N. Muroyama for fruitful discussions. This work was financially supported by a Grant-in-Aid for Scientific Research (B) 24360318 from MEXT.

References

Agrawal, R., Kofke, D.A.: Thermodynamic and structural-properties of model systems at solid–fluid coexistence. 2. Melting and sublimation of the Lennard-Jones system. Mol. Phys. **85**, 43–59 (1995)

Bakaev, V.A., Steele, W.A., Bakaeva, T.I., Pantano, C.G.: Adsorption of CO_2 and Ar on glass surfaces. Computer simulation and experimental study. J. Chem. Phys. **111**, 9813–9821 (1999)

Bhattacharya, S., Coasne, B., Hung, F.R., Gubbins, K.E.: Modeling micelle-templated mesoporous material SBA-15: atomistic model and gas adsorption studies. Langmuir **25**, 5802–5813 (2009)

Ciesla, U., Schuth, F.: Ordered mesoporous materials. Microprous Mesoporous Mater. **27**, 131–149 (1999)

Coasne, B., Pellenq, R.J.M.: Grand canonical Monte Carlo simulation of argon adsorption at the surface of silica nanopores: effect of pore size, pore morphology, and surface roughness. J. Chem. Phys. **120**, 2913–2922 (2004a)

Coasne, B., Pellenq, R.J.M.: A grand canonical Monte Carlo study of capillary condensation in mesoporous media: effect of the pore morphology and topology. J. Chem. Phys. **121**, 3767–3774 (2004b)

Coasne, B., Ugliengo, P.: Atomistic model of micelle-templated mesoporous silicas: structural, morphological, and adsorption properties. Langmuir **28**, 11131–11141 (2012)

Coasne, B., Galarneau, A., Di Renzo, F., Pellenq, R.J.M.: Gas adsorption in mesoporous micelle-templated silicas: MCM-41, MCM-48, and SBA-15. Langmuir **22**, 11097–11105 (2006a)

Coasne, B., Hung, F.R., Pellenq, R.J.M., Siperstein, F.R., Gubbins, K.E.: Adsorption of sample gases in MCM-41 materials: the role of surface roughness. Langmuir **22**, 194–202 (2006b)

Coasne, B., Galarneau, A., Di Renzo, F., Pellenq, R.J.M.: Effect of morphological defects on gas adsorption in nanoporous silicas. J. Phys. Chem. C **111**, 15759–15770 (2007)

Coasne, B., Di Renzo, F., Galarneau, A., Pellenq, R.J.M.: Adsorption of simple fluid on silica surface and nanopore: effect of surface chemistry and pore shape. Langmuir **24**, 7285–7293 (2008a)

Coasne, B., Galarneau, A., Di Renzo, F., Pellenq, R.J.M.: Molecular simulation of adsorption and intrusion in nanopores. Adsorption **14**, 215–221 (2008b)

Coasne, B., Galarneau, A., Di Renzo, F., Pellenq, R.J.M.: Molecular simulation of nitrogen adsorption in nanoporous silica. Langmuir **26**, 10872–10881 (2010)

Corma, A.: From microporous to mesoporous molecular sieve materials and their use in catalysis. Chem. Rev. **97**, 2373–2419 (1997)

Edler, K.J., Reynolds, P.A., White, J.W., Cookson, D.: Diffuse wall structure and narrow mesopores in highly crystalline MCM-41 materials studied by X-ray diffraction. J. Chem. Soc. Faraday Trans. **93**, 199–202 (1997)

Gelb, L.D., Gubbins, K.E., Radhakrishnan, R., Sliwinska-Bartkowiak, M.: Phase separation in confined systems. Rep. Prog. Phys. **62**, 1573–1659 (1999)

Gommes, C.J., Friedrich, H., Wolters, M., de Jongh, P.E., de Jong, K.P.: Quantitative characterization of pore corrugation in ordered mesoporous materials using image analysis of electron tomograms. Chem. Mater. **21**, 1311–1317 (2009)

He, Y.F., Seaton, N.A.: Experimental and computer simulation studies of the adsorption of ethane, carbon dioxide, and their binary mixtures in MCM-41. Langmuir **19**, 10132–10138 (2003)

Hofmann, T., Wallacher, D., Huber, P., Birringer, R., Knorr, K., Schreiber, A., Findenegg, G.H.: Small-angle X-ray diffraction of Kr in mesoporous silica: effects of microporosity and surface roughness. Phys. Rev. B **72**, 064122-1–064122-7 (2005)

Hung, F.R., Bhattacharya, S., Coasne, B., Thommes, M., Gubbins, K.E.: Argon and krypton adsorption on templated mesoporous silicas: molecular simulation and experiment. Adsorption **13**, 425–437 (2007)

Imperor-Clerc, M., Davidson, P., Davidson, A.: Existence of a microporous corona around the mesopores of silica-based SBA-15 materials templated by triblock copolymers. J. Am. Chem. Soc. **122**, 11925–11933 (2000)

Kanda, H., Miyahara, M., Higashitani, K.: Condensation model for cylindrical nanopores applied to realistic porous glass generated by molecular simulation. Langmuir **16**, 6064–6066 (2000a)

Kanda, H., Miyahara, M., Yoshioka, T., Okazaki, M.: Verification of the condensation model for cylindrical nanopores. Analysis of the nitrogen isotherm for FSM-16. Langmuir **16**, 6622–6627 (2000b)

Kresge, C.T., Leonowicz, M.E., Roth, W.J., Vartuli, J.C., Beck, J.S.: Ordered mesoporous molecular-sieves synthesized by a liquid-crystal template mechanism. Nature **359**, 710–712 (1992)

Maddox, M.W., Olivier, J.P., Gubbins, K.E.: Characterization of MCM-41 using molecular simulation: heterogeneity effects. Langmuir **13**, 1737–1745 (1997)

Miyahara, M., Kanda, H., Yoshioka, T., Okazaki, M.: Modeling capillary condensation in cylindrical nanopores: a molecular dynamics study. Langmuir **16**, 4293–4299 (2000)

Miyasaka, K., Neimark, A.V., Terasaki, O.: Density functional theory of in situ synchrotron powder X-ray diffraction on mesoporous crystals: argon adsorption on MCM-41. J. Phys. Chem. C **113**, 791–794 (2009)

Monson, P.A.: Understanding adsorption/desorption hysteresis for fluids in mesoporous materials using simple molecular models and classical density functional theory. Microporous Mesoporous Mater. **160**, 47–66 (2012)

Morishige, K., Ishino, M.: Lower closure point of adsorption hysteresis in ordered mesoporous silicas. Langmuir **23**, 11021–11026 (2007)

Morishige, K., Ito, M.: Capillary condensation of nitrogen in MCM-41 and SBA-15. J. Chem. Phys. **117**, 8036–8041 (2002)

Morishige, K., Nakamura, Y.: Nature of adsorption and desorption branches in cylindrical pores. Langmuir **20**, 4503–4506 (2004)

Morishige, K., Fujii, H., Uga, M., Kinukawa, D.: Capillary critical point of argon, nitrogen, oxygen, ethylene, and carbon dioxide in MCM-41. Langmuir **13**, 3494–3498 (1997)

Muroyama, N., Ohsuna, T., Ryoo, R., Kubota, Y., Terasaki, O.: An analytical approach to determine the pore shape and size of MCM-41 materials from X-ray diffraction data. J. Phys. Chem. B **110**, 10630–10635 (2006)

Muroyama, N., Yoshimura, A., Kubota, Y., Miyasaka, K., Ohsuna, T., Ryoo, R., Ravikovitch, P.I., Neimark, A.V., Takata, M., Terasaki, O.: Argon adsorption on MCM-41 mesoporous crystal studied by in situ synchrotron powder X-ray diffraction. J. Phys. Chem. C **112**, 10803–10813 (2008)

Neimark, A.V., Vishnyakov, A.: Gauge cell method for simulation studies of phase transitions in confined systems. Phys. Rev. E **62**, 4611–4622 (2000)

Neimark, A.V., Ravikovitch, P.I., Vishnyakov, A.: Adsorption hysteresis in nanopores. Phys. Rev. E **62**, R1493–R1496 (2000)

Neimark, A.V., Ravikovitch, P.I., Vishnyakov, A.: Bridging scales from molecular simulations to classical thermodynamics: density functional theory of capillary condensation in nanopores. J. Phys. Condens. Matter **15**, 347–365 (2003)

Peterson, B.K., Gubbins, K.E.: Phase-transitions in a cylindrical pore—grand canonical Monte-Carlo, mean field-theory and the Kelvin equation. Mol. Phys. **62**, 215–226 (1987)

Peterson, B.K., Walton, J., Gubbins, K.E.: Fluid behavior in narrow pores. J. Chem. Soc. Faraday Trans. **II**(82), 1789–1800 (1986)

Ravikovitch, P.I., Neimark, A.V.: Density functional theory model of adsorption on amorphous and microporous silica materials. Langmuir **22**, 11171–11179 (2006)

Ravikovitch, P.I., Vishnyakov, A., Neimark, A.V.: Density functional theories and molecular simulations of adsorption and phase transitions in nanopores. Phys. Rev. E **64**, 011602-1–011602-20 (2001)

Ravikovitch, P.I., Odomhnaill, S.C., Neimark, A.V., Schuth, F., Unger, K.K.: Capillary hysteresis in nanopores: theoretical and experimental studies of nitrogen adsorption on MCM-41. Langmuir **11**, 4765–4772 (1995)

Ravikovitch, P.I., Haller, G.L., Neimark, A.V.: Density functional theory model for calculating pore size distributions: pore structure of nanoporous catalysts. Adv. Colloid Interface Sci. **76**, 203–226 (1998)

Rosenfeld, Y.: Free-energy model for the inhomogeneous hard-sphere fluid mixture and density-functional theory of freezing. Phys. Rev. Lett. **63**, 980–983 (1989)

Schumacher, C., Gonzalez, J., Wright, P.A., Seaton, N.A.: Generation of atomistic models of periodic mesoporous silica by kinetic Monte Carlo simulation of the synthesis of the material. J. Phys. Chem. B **110**, 319–333 (2006)

Siperstein, F.R., Gubbins, K.E.: Phase separation and liquid crystal self-assembly in surfactant-inorganic-solvent systems. Langmuir **19**, 2049–2057 (2003)

Soler-Illia, G.J.D., Sanchez, C., Lebeau, B., Patarin, J.: Chemical strategies to design textured materials: from microporous and mesoporous oxides to nanonetworks and hierarchical structures. Chem. Rev. **102**, 4093–4138 (2002)

Sonwane, C.G., Jones, C.W., Ludovice, P.J.: A model for the structure of MCM-41 incorporating surface roughness. J. Phys. Chem. B **109**, 23395–23404 (2005)

Tarazona, P.: Free-energy density functional for hard-spheres. Phys. Rev. A **31**, 2672–2679 (1985)

Tarazona, P., Marconi, U.M.B., Evans, R.: Phase-equilibria of fluid interfaces and confined fluids—nonlocal versus local density functionals. Mol. Phys. **60**, 573–595 (1987)

Vanbeest, B.W.H., Kramer, G.J., Vansanten, R.A.: Force-fields for silicas and aluminophosphates based on abinitio calculations. Phys. Rev. Lett. **64**, 1955–1958 (1990)

Vishnyakov, A., Neimark, A.V.: Studies of liquid–vapor equilibria, criticality, and spinodal transitions in nanopores by the gauge cell Monte Carlo simulation method. J. Phys. Chem. B **105**, 7009–7020 (2001)

Zhao, D.Y., Feng, J.L., Huo, Q.S., Melosh, N., Fredrickson, G.H., Chmelka, B.F., Stucky, G.D.: Triblock copolymer syntheses of mesoporous silica with periodic 50 to 300 angstrom pores. Science **279**, 548–552 (1998)